Novel Clay-Based Nanobiocomposites of Biopolyesters with Synergistic Barrier to UV Light, Gas, and Vapour

M. D. Sanchez-Garcia, J. M. Lagaron

Novel Materials and Nanotechnology Lab., IATA, CSIC, Burjassot 46100, Spain

Received 6 August 2009; accepted 16 December 2009
DOI 10.1002/app.31986
Published online 19 May 2010 in Wiley InterScience (www.interscience.wiley.com).

ABSTRACT: This article presents novel solvent cast biocomposites of poly(lactic acid) (PLA), polyhydroxybutyrate-*co*-valerate (PHBV), and polycaprolactone (PCL) with enhanced barrier properties to UV light, oxygen, water, and limonene by means of incorporating an organomodified mica-based clay grade. The TEM results suggested a good clay dispersion but with no exfoliation in the three biopolyesters. In agreement with the crystallinity data, which was found to generally increase with increasing filler content, oxygen but specially water and D-limonene permeability coefficients were seen to decrease to a significant extent in the biocomposites and an optimum property balance was found for 5 wt % of clay loading in the three biopolymers. With increasing clay content, the light transmission of these biodegradable biocomposites decreased by up to 90% in the UV wavelength region due to the specific UV blocking nature of the clay used. As a result, these new biocomposites can have significant potential to develop packaging films, coatings and membranes with enhanced gas and vapor barrier properties and UV blocking performance.
 J Appl Polym Sci 118: 188–199, 2010

Key words: clay-based composites; packaging; barrier properties; biopolyesters

INTRODUCTION

Protection against light is a basic requirement to preserve the quality of many products, such as packaged foods. Metal and paper being opaque to the transmission of light, automatically provide this function. On the other hand, plastic films are often transparent materials to UV and Visible radiation of short wavelengths. Therefore, the protection of light sensitive goods, such as fruit and vegetable juices, vitamin and sport drinks, dairy products, and edible oils from UV-radiation when packaged in plastic containers has been widely investigated.[1–3]

The primary wavelengths of interest in, for instance, food packaging applications are those that fall between 200 and 2200 nm. This section of the electromagnetic spectrum can be divided into three components: the ultraviolet (UV) range (100–400 nm); the visible spectrum (400–700 nm); and the near-infrared range (700–2200 nm). Ultraviolet radiation accounts for only 3% of the total radiation that reaches earth, but it causes chemical reactions, weathering of polymers, fading of certain coloring, and even eye and skin damage. For this reason, UV light blocking is a very demanded property in polymers and also in the newcoming renewable and biodegradable polymers of interest in multisectorial applications.

Biodegradable and/or sustainable materials present a number of excellent properties for a number of applications, including packaging, automotive, and biomedical fields. Thermoplastic biopolymers, such as poly(lactic acid) (PLA), polyhydroxyalkanoates (PHA), and polycaprolactones (PCL), exhibit an excellent balance between barrier and mechanical properties, are water resistant and can be processed using conventional plastics machinery. Moreover, for the case of the first two, they originate from renewable resources, i.e., maize and microorganisms, respectively. Composites of biopolymers, often called nanobiocomposites, containing highly dispersed naturally derived layered additives, typically montmorillonite (MMT), are proving to be an excellent technology to design new materials with enhanced key properties while retaining the "bio" characteristics. Nanocomposites of biodegradable materials containing between 1 and 5 wt % of MMT have been claimed to exhibit significant improvements in barrier[4–9] and in mechanical properties[10,11]

Correspondence to: J. M. Lagaron (lagaron@iata.csic.es).
Contract grant sponsor: Spanish MEC project; contract grant number: MAT2006-10261-C03.
Contract grant sponsor: Spanish CONSOLIDER project FUN-C-FOOD; contract grant number: CSD2007-00063.
Contract grant sponsor: FPI program (GV associated to the MEC project); contract grant number: MAT2003-08480-C3.
Contract grant sponsor: NanoBioMatters S.L. (Paterna, Spain).

and have been reported to be able to disperse to a very little amount the UV-visible radiation,[12] probably due to the reduced scattering phenomena caused by the highly dispersed clay nanolayers. Petersson et al.[12] also reported some reduction of the light transmitted by nanocomposites of PLA containing 5 wt % of MMT compared to pure PLA.

Nevertheless, the development of clay-based nanocomposites in packaging has always been aimed at minimizing the impact of the filler in the optical properties, i.e. in transparency, of the polymer matrix. To study this UV-Vis characterization of nanocomposites has previously being carried out in the existing literature. Thus, some earlier works reported by UV-Vis spectroscopy the impact in optical properties of polymer nanocomposites based in MMT containing between 3 and 10% of the clay inside petroleum-derived polymers, such as nylon,[13] polyimide,[14] PVC,[15] polyvinyl alcohol,[16,17] and other commodities.[18] There are also other works, which reported some reduction of the UV-Vis transmission in polyvinyl alcohol containing between 0.5–10 wt % content of Red Mud[19] and also in PMMA containing 1 to 5 wt % content of 10-undecenoate intercalated layered double hydroxides.[20] In spite of this, there is no previous literature regarding the use of clay based systems as an intended route to generate UV blocking properties in films or coatings and neither was the study of mica-based clays to enhance the overall barrier properties of bioplastics.

In this study, the morphology, UV-Vis blocking efficiency, color, and gas and vapor barrier properties as a function of clay content of novel mica-based biocomposites of solvent cast PLA, PCL, and PHBV are presented and discussed.

MATERIALS AND METHODS

Materials

The bacterial polyhydroxyalcanoate grade was purchased from Goodfellow Cambridge Limited, U.K., in pellet form. The supplied material was a melt-processable semicrystalline thermoplastic PHBV (polyhydroxybutyrate with 12 mol % of valerate) copolymer made by biological fermentation from renewable carbohydrate feedstocks. The PCL grade FB100 was kindly supplied in pellet form by Solvay Chemicals, Belgium. This grade has a density of 1.1 g/cm^3 and a mean molecular weight of 100,000 g/mol. The semicrystalline PLA used was a film extrusion grade produced by Natureworks (with a D-isomer content of approximately 2%). The molecular weight had a number-average molecular weight (M_n) of ca. 130,000 g/mol, and the weight-average molecular weight (M_w) was ca. 150,000 g/mol.

A proprietary food contact commercial laminar phyllosilicate grade termed NanoBioTer® AC11 based on a mica (so-called through the paper clay) containing 30 wt % (as determined by TGA) of an organophilic modification was kindly supplied in powder form by NanoBioMatters, Paterna, Spain. The clay grade was characterized to be a very fine slightly brown powder and no further details of sample preparation and modification were disclosed by the manufacturer.

Preparation of blends

Before to the mixing step, the PHBV, PLA, and the filler were dried at 70°C and the PCL at 45°C under vacuum for 24 h to remove sorbed moisture.

Solution-cast film samples of the biodegradable materials containing 1, 5, and 10 wt % of the clay filler were prepared with a dry film thickness of around 100 μm, using chloroform as a solvent. Organoclay solutions in chloroform were heavily mixed using a homogenizer (Ultraturrax T25 basic, Ika-Werke, Germany) for 5 min and were then stirred with the polymer at 40°C during 30 min and subsequently cast onto Petri dishes to generate films after solvent evaporation at room temperature conditions.

Transmission electron microscopy measurements

Transmission electron microscopy (TEM) was performed using a JEOL 1010 (Jeol, Tokyo, Japan) equipped with a digital Bioscan (Gatan) image acquisition system. TEM observations were performed on ultra-thin sections of microtomed thin biocomposite sheets and collected over a water pool. The PCL specimens could not be successfully cut to generate clear TEM observations due to the high plasticity of the material even when cryogenic cutting conditions were used.

AFM measurements

AFM measurements were performed on PCL composites using an Agilent 5500 SPM system (provided by Scientec Ibérica, Spain) to investigate the morphology of the composite surfaces on both sides of the cast films. The images were scanned in tapping mode in air using commercial Si cantilevers with a resonance frequency of 320 kHz.

DSC measurements

Differential scanning calorimetry (DSC) of PCL, PHBV, and PLA and its composites was performed on a Perkin-Elmer DSC 7 thermal analysis system on typically 7 mg of material at a scanning speed of 10°C/min from room temperature to the melting

point of these materials. The thermograms were corrected with these of an empty pan and the DSC equipment was calibrated with an indium standard. To calculate the heat of fusion of the PLA the enthalpy of the melting peak was subtracted the enthalpy of the cold crystallization peak. Crystallinity was estimated using the ratio between the heat of fusion of the studied material and the heat of fusion of an infinity crystal of same material, i.e.

$$\%X_c = \frac{\Delta H_f}{\Delta H_f^0} \times 100, \quad (1)$$

where ΔH_f is the enthalpy of fusion of the studied specimen and ΔH_f^0 is the enthalpy of fusion of a totally crystalline material. The ΔH_f^0 used was 93 J/g for PLA,[21] 146 J/g for PHBV,[22] and 136 J/g for PCL [7].

UV-VIS spectra

An UV–Vis spectrophotometer (Hewlett Packard 8452A Diode Array Spectropotometer) was used to measure the transmittance spectra of specially prepared thin films in the wavelength range 200–700 nm. Thin films of biodegradable materials and their composites of ca. 30 microns were specially prepared by casting over the surface of quartz cuvettes typically in UV-Vis. In all cases, the UV abortion signal of the films was normalized to exactly 30 microns of thickness for comparative purposes.

The yellow index (YI) was calculated from the transmittance values of the UV-Vis spectra. The YI was calculated using the following relationship[18]:

$$YI = \frac{T_{680} - T_{420}}{T_{560}} \quad (2)$$

where T_{680}, T_{420}, and T_{560} are the transmission dates at the wavelength of 680 nm, 420 nm, and 560 nm, respectively.

Color measurements

Color parameters were determined in the reflective mode using a colorimeter, Minolta Chroma Meter CR-300 series.

Gravimetric measurements

Direct permeability to D(+)-limonene of 95% purity (Panreac Química, Spain) and direct permeability to water were determined from the slope of weight loss vs. time experiments at 24°C and 40%RH. The films were sandwiched between the aluminum top (open O-ring) and bottom (deposit for the permeant) parts of aluminum permeability cells. A Viton rubber O-ring was placed between the film and the bottom part of the cell to enhance sealability. Then the bottom part of the cell was filled with the permeant and the pinhole secured with a rubber O-ring and a screw. Finally, the cell was placed in the desired environment and the solvent weight loss through a film area of 0.001 m^2 was monitored and plotted as a function of time. Cells with aluminum films (with thickness of ca. 100 microns) were used as control samples to estimate solvent loss through the sealing. The permeability sensibility of the permeation cells was determined to be of ca. 0.01 10^{-13} Kg m/s m^2 Pa based on the weight loss measurements of the aluminum cells. Cells clamping polymer films but with no solvent were used as blank samples to monitor water uptake. Solvent permeation rates were estimated from the steady-state permeation slopes. Water vapor weight loss was calculated as the total cell loss minus the loss through the sealing. Organic vapor weight loss was calculated as the total cell loss minus the loss through the sealing and plus the water weight gain. The tests were done in duplicate for both permeants.

Oxygen transmission rate

The oxygen permeability coefficient was derived from oxygen transmission rate (OTR) measurements recorded using an Oxtran 100 equipment (Modern Control, Minneapolis, MN, US). During all experiments temperature and relative humidity were held at 24°C and 80% R.H. 80% relative humidity was generated by a built in gas bubbler and was checked with a hygrometer placed at the exit of the detector. The experiments were done in duplicate. The samples were purged with nitrogen for a minimum of 20 h before exposure to a 100% oxygen flow of 10 mL/min, and a 5 cm^2 sample area was measured by using an in-house developed mask. Permeability (P) was estimated from fitting the OTR-time curve to the first six sum terms of the following solution of the Fick's second law[23]:

$$OTR(t) = \frac{P_p}{l}\left[1 + 2\sum_{n=1}^{\infty}(-1)^n \exp\left(-\frac{D\pi^2 n^2 t}{l^2}\right)\right] \quad (3)$$

In eq. (1), D is the diffusion coefficient, p is the oxygen partial pressure, and l is the film thickness.

RESULTS AND DISCUSSION

Biocomposites morphology

Figure 1 shows typical pictures of PLA and PLA biocomposite films containing 1, 5, and 10 wt % of the clay. From these pictures, it can be seen that while all samples remain transparent at 100 microns

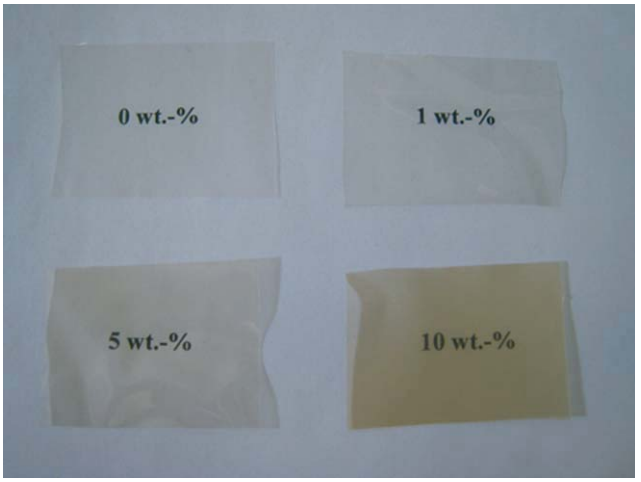

Figure 1 Typical photographs of 100 microns thickness films of PLA and of PLA containing 1, 5, and 10 wt % of clay. [Color figure can be viewed in the online issue, which is available at www.interscience.wiley.com.]

thickness, specially the PLA and PLA+1 wt % clay, the biocomposites exhibit a brownish color with increasing clay content due to the presence of this particular filler in the matrix.

Figure 2 shows some TEM images taken in specimens of composites of PHBV, and PLA. The PCL cuts were too thick and exhibited many wrinkles, which made not possible to unambiguously discern the clay morphology. In Figure 2, the PLA and PHBV specimens show a dispersed clay morphology with long platelets, in which a considerable reduction of the original tactoid size is attained in the thickness direction. In any case, no exfoliation was observed for the samples. Notwithstanding the above, most layered particles, particularly the PHBV composites, are below 100 nm in thickness, typical upper size limit definition for a nanotech product. The remarkable observation from Figure 2, is the extremely large length of the platelets dispersed in the matrix. Filler dispersion seems higher for PHBV than for PLA and the particles appeared rather oriented. In any case, it is clear that the solution casting method used does not lead to exfoliated morphologies, which are seldom obtained irrespective of the processing method, but still yields interesting nanobiocomposites with enhanced properties as it will be shown later in the article. Particle size and dispersion seem better for PHBV than for PLA, and in all cases are well below the micron in the thickness direction. Fractured particles along the layered axis are also observed due to the potentially aggressive homogenization processed applied.

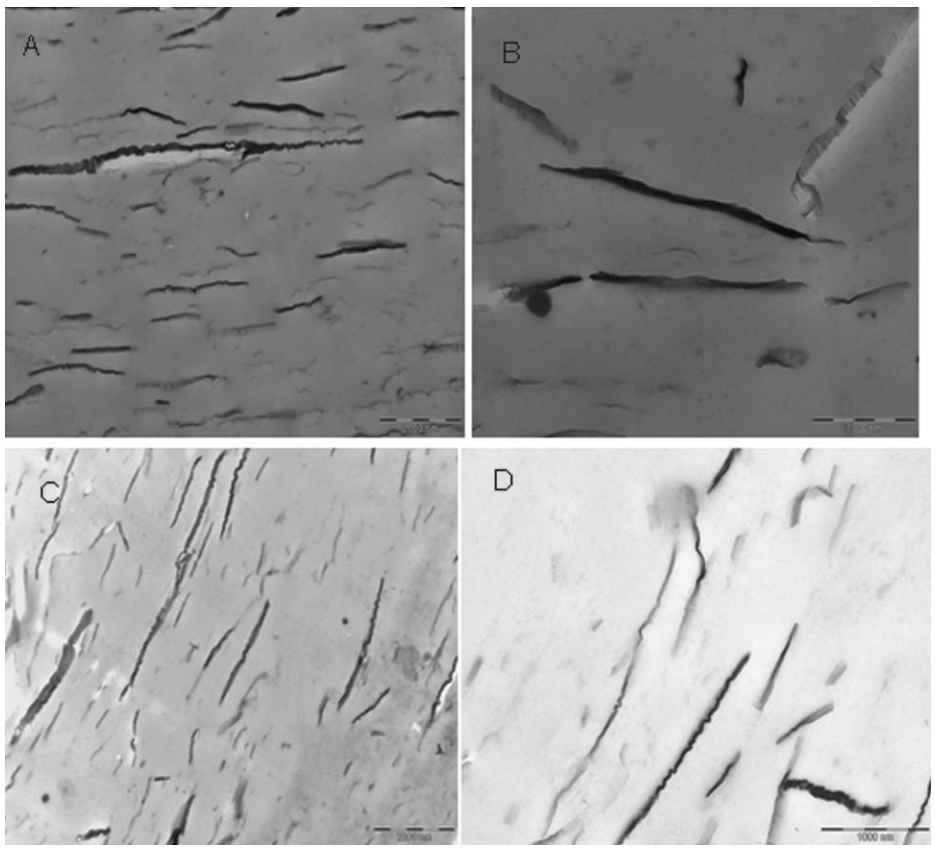

Figure 2 TEM pictures of (A) and (B) PLA containing 5 wt % of clay and (C) and (D) PHBV containing 5 wt % of clay. Scale markers are 2000 nm for the left pictures and 1000 nm for the right pictures.

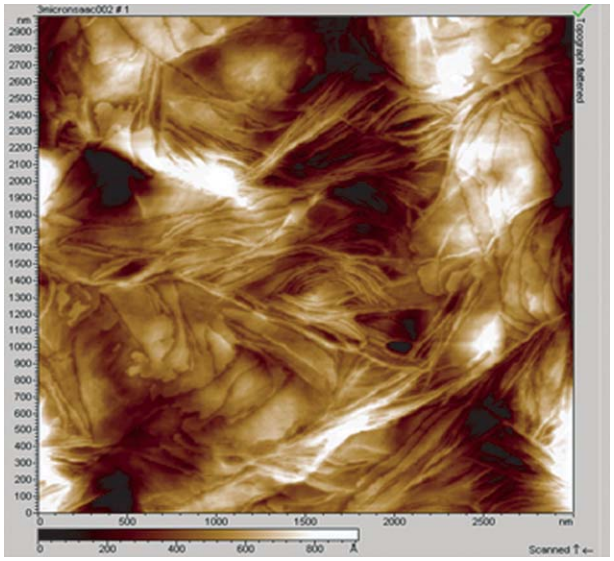

Figure 3 AFM topography picture of the 5 wt % clay PCL biocomposite. [Color figure can be viewed in the online issue, which is available at www.interscience.wiley.com.]

Figure 3 shows the surface roughness by AFM (topographic image) of the PCL cast composite sample containing 5 wt % of clay content. The image suggests that the extremely large particles are intercalated by the polymer and are greatly dispersed within this biopolymer matrix. This Figure also suggests that there appears to be a good adhesion of the filler to the biopolymer, this is most likely promoted by the hydrophobic surface modification of the filler. Regarding particle thickness, the clay layers exhibit typical thicknesses around 16 nm.

Thermal properties

Melting temperature (T_m) and heat of fusion (ΔH_m) corrected for biopolymer content in the biocomposites were determined from the DSC thermograms of the samples. Figure 4 shows some typical first melting endotherms of the neat biopolymers and of the 5 wt % filler loaded biocomposites. Data from the first and the second heating runs are summarized in Table I for cast films of PCL with different clay filler contents. The first heating run is related to the original state of the material after solvent casting and is,

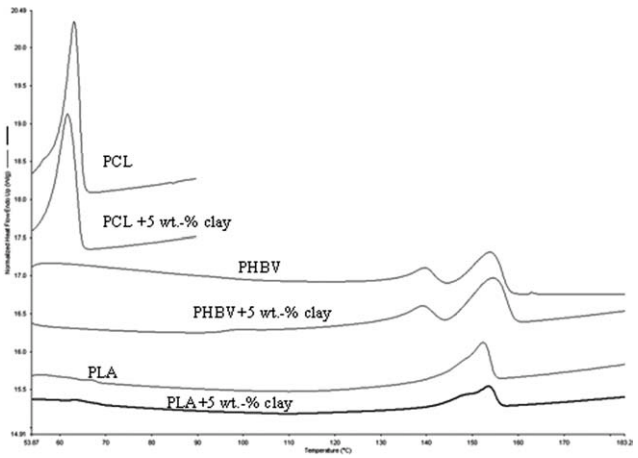

Figure 4 Normalized for total mass typical DSC thermographs of the biopolymers PCL, PHBV, and PLA and their biocomposites with 5 wt % clay in the first heating run.

therefore, more meaningful for correlation with physical properties, such as mass transfer properties. From this Table I, the heat of fusion of PCL and, therefore, the crystallinity is seen to increase in the biocomposite during the first heating run of this biomaterial but the melting point is largely unmodified or changes very slightly, i.e. it drops by ca. 1°C in the 5 wt % loaded composite. The latter results add to similar nucleating observations reported in previous works for PHB/PCL nanocomposites,[7] and suggest that the clay can act as a heterophase nucleating agent, hence promoting higher molecular order in the matrix. The second heating run shows lower values for both melting temperature and heat of fusion compared to the first run, due to possibly faster cooling and higher metastability compared to the solvent casting method. Table I also shows that the values for the second heating run have the same comparative behavior as for the first heating run.

Table II summarizes melting temperature (T_m), heat of fusion (ΔH_m), and the crystallization temperature (T_c) of the PHBV and of their biocomposites during the first and second heating runs. From this table, it can be seen that in the first heating run, the melting point is not greatly altered in the clay containing samples but it is slightly increased for the 5 wt % loaded composite. However, in the second heating run the melting point decreases with

TABLE I
DSC Melting Point, Melting Enthalpy, and Crystallinity (%Xc) of PCL and of PCL biocomposites containing 1, 5, and 10 wt % of clay

Sample	T_m (°C) 1st heating	ΔH_m (J/g) 1st heating	$\%X_c$ 1st heating	T_m (°C) 2nd heating	ΔH_m (J/g) 2nd heating
PCL	63.25 ± 0.09	51.82 ± 0.05	38	55.75 ± 0.09	38.49 ± 3.85
PCL+1 wt %	63.09 ± 0.19	55.89 ± 1.26	41	55.94 ± 0.12	41.07 ± 0.97
PCL+5 wt %	61.92 ± 0.38	57.92 ± 1.28	42	55.86 ± 0.16	41.90 ± 4.44
PCL+10 wt %	63.75 ± 0.96	65.06 ± 0.75	48	55.78 ± 0.12	42.80 ± 2.89

increasing clay content up to about 16°C due to possibly clay-induced polymer degradation, both hydrolytic and adiabatic.[7,24] During the first and second heating runs, the melting enthalpy (corrected for the biopolymer content in the composite) decreases somewhat at low clay contents (1 wt %), however at 5 wt % of clay content, the enthalpy of fusion is the highest in the concentration range screened. In spite of this, filler-induced crystallinity changes are very small for this biopolymer. The crystallization temperature is also not altered in the clay containing samples, except for the 5 wt % of clay, where the crystallization increases by 4°C.

The thermal behavior of PLA is different and more complex than that of the two previous biopolyesters, because PLA exhibits a cold crystallization process[25] similar to that typically observed for the petroleum-based polyester polyethylene terephthalate (PET). Table III gathers the melting temperature (T_m), heat of fusion (ΔH_m), and the cold crystallization temperature (T_{cc}) of PLA and of their biocomposites after the first and second heating runs. From this Table III, the heat of fusion in the first and second endotherms is seen to increase in the biocomposites. The melting point remains largely unmodified albeit it increases slightly in the 5 wt % filler loaded composite. A curious observation from this Table III is that while the neat PLA does not have a measurable melting endotherm in the second heating, so the polymer is in an amorphous state, the PLA biocomposites exhibit some crystallinity. This suggests again that the clay acts as a nucleating agent for the polymer. However, from Table III, the cold crystallization temperature increases particularly for the highest filler content, suggesting that the clay does in fact delay the cold crystallization process upon heating.

Table III also shows that the T_g of these biocomposites increases slightly with filler content, due to possibly clay-induced stiffening of the biopolymer amorphous phase. However, for the film of PLA with 10 wt % of clay the T_g increase is less pronounced than for the composites containing 1 and 5 wt. % of clay. The reason for not observing a higher T_g rise in the samples with the highest filler loading must be attributed to further inefficiency of the clay as a reinforcing element due to clay extensive segregation and agglomeration.

In summary, the clay has a generic role in the biocomposites thermal properties, of nucleation and promotion of some crystallinity, particularly for PCL and PLA. In principle, filler-induced crystallization of the biopolymers is positive from a barrier perspective, as crystals are typically impermeable systems to the transport of low molecular weight compounds. Nevertheless, extensive crystallization may also promote, as a downside, excessive rigidity and

TABLE II
DSC Melting Point and Melting Enthalpy During the first and second Heating Runs and Crystallization Temperature of PHBV and of PHBV Biocomposites with 1, 5, and 10 wt % Clay Content

Sample	T_m (°C) 1st heating	ΔH_m (J/g) 1st heating	$\%X_c$ 1st heating	T_m (°C) 2nd heating	ΔH_m (J/g) 2nd heating	T_c (°C)
PHBV	(139.86–153.87) ± (0.23–0.00)	35.17 ± 0.95	24	(146.45–157.28) ± (0.11–0.12)	37.42 ± 0.87	93.63 ± 0.70
PHBV+1 wt %	(138.85–152.94) ± (1.20–1.31)	32.95 ± 2.56	22	(143.45–153.45) ± (0.11–1.76)	37.23 ± 2.03	92.89 ± 0.58
PHBV+5 wt %	(138.86–154.28) ± (0.23–0.35)	39.33 ± 4.70	27	(140.45–150.95) ± (1.30–1.06)	39.14 ± 6.97	97.22 ± 0.35
PHBV+10 wt %	(138.53–154.20) ± (0.47–0.82)	37.71 ± 2.10	26	(130.70–143.37) ± (1.88–1.41)	35.47 ± 0.40	90.13 ± 0.94

TABLE III
DSC Melting Point, Melting Enthalpy, Cold Crystallization Temperature, and T_g During the First and Second Heating Runs of PLA and of PLA Biocomposites Containing 1, 5, and 10 wt % of clay

Sample	T_m (°C) 1st heating	ΔH_m (J/g) 1st heating	T_{cc} (°C) 1st heating	$\%X_c$ 1st heating	T_m (°C) 2nd heating	ΔH_m (J/g) 2nd heating	T_{cc} (°C) 2nd heating	T_g (°C) 2nd heating
PLA	152.53 ± 0.23	8.51 ± 1.61	110.95 ± 1.30	9.1	–	–	–	59.06 ± 0.31
PLA+1 wt. %	153.09 ± 0.25	10.87 ± 0.69	110.14 ± 0.78	11.6	151.70 ± 0.24	4.87 ± 2.20	127.20 ± 0.23	59.33 ± 0.48
PLA+5 wt. %	153.45 ± 0.11	10.86 ± 0.82	109.7 ± 1.41	11.6	151.78 ± 0.35	4.42 ± 0.87	125.95 ± 0.82	63.01 ± 4.88
PLA+10 wt. %	151.86 ± 1.18	16.90 ± 3.04	116.7 ± 7.78	18.1	151.36 ± 1.64	13.14 ± 2.02	126.70 ± 3.07	60.13 ± 0.23

hence fragility for the biopolymer mechanical performance.

Mass transport properties

Table IV gathers the water, limonene, and oxygen permeability coefficients of the materials and of their biocomposites. A curious first observation from Table IV regarding PCL is that the water permeability coefficient of 3.39 10^{-14} Kg m/s m^2 Pa is much higher than that of 0.023 10^{-14} Kg m/s m^2 Pa previously reported for toluene cast PCL.[8] The reason for the large disagreement could be related to the different origin of the two samples (lab scale material vs. industrial scale material production) and the fact that molecular weight, the solvent used and the differences in relative humidity gradient used for testing were totally different. Direct permeability for limonene in PLA was not reported, because the measurements yielded values below the sensitivity of the permeation method used; nevertheless, a previous study reported that the limonene permeability for PLA is of ca. 0.000002 10^{-13} Kg m/s m^2 Pa when measured at 45°C and 258 Pa of vapor partial pressure gradient.[26] The previously reported water direct permeability of 1.80 10^{-14} Kg m/s m^2 Pa for PLA films using chloroform as a solvent is, on the other hand, very similar to the one measured in our laboratory, due to the similar conditions of the film produced.

Figure 5(A) shows the plot of the water permeability of the neat PLA, PHBV, and PCL and of their biocomposites with 1, 5, and 10 wt % of clay content. In the case of PLA, reductions of water permeability of ca. 27, 54, and 55% were obtained for the cast films containing 1, 5 and 10 wt % of clay, respectively. The barrier improvement for the samples containing 5 and 10 wt % of clay content yielded similar barrier. Water barrier also increased with increasing clay content. In the case of PHBV, the film containing 1 wt % of clay shows a water permeability reduction of 61%, the one containing 5 wt % of clay shows a reduction of ca. 76%, but for the film PHBV+10 wt % of clay the reduction is of ca. 47%. In this case of the film containing 10 wt % of clay the water permeability reduction was lower than for films with 1 and 5 wt % filler content, possibly due to the clay content surpassing the solubility limit and hence resulting in detrimental agglomeration. For the case of PCL composites, films of this biodegradable polymer containing 1, 5, and 10 wt % clay exhibit a water permeability decrease of 54, 63, and 63%, respectively, compared to the unfilled material. The latter results are similar in trend to those of PLA.

Figure 5(B) shows the limonene permeability for neat PHBV and PCL and their biocomposites. In the

TABLE IV
Water, Limonene, and Oxygen Permeability Coefficients of PLA, PHBV, PCL, and their biocomposites

	P_{water} (Kg m/s m^2 Pa)	$P_{limonene}$ (Kg m/s m^2 Pa)	P_{oxygen} (m^3 m/s m^2 Pa) at 80%RH
PLA	$2.30 \pm 0.07e^{-14}$	–	$2.77 \pm 0.08e^{-18}$
PLA+1 wt %	$1.69 \pm 0.07e^{-14}$	–	$2.08 \pm 0.16e^{-18}$
PLA+5 wt %	$1.05 \pm 0.26e^{-14}$	–	$1.24 \pm 0.20e^{-18}$
PLA+10 wt %	$1.03 \pm 0.11e^{-14}$	–	$1.09 \pm 0.17e^{-18}$
Literature value PLA	[27] $1.26\ e^{-14}$	–	[28b] $1.75e^{-18}$
Literature value PLA	[29] $1.80e^{-14}$		
PHBV	$1.27 \pm 0.14e^{-14}$	$1.27 \pm 0.07e^{-13}$	$1.44 \pm 0.01e^{-18}$
PHBV+1 wt %	$0.49 \pm 0.03e^{-14}$	$0.72 \pm 0.23e^{-13}$	$1.53 \pm 0.01e^{-18}$
PHBV+5 wt %	$0.30 \pm 0.09e^{-14}$	$0.28 \pm 0.04e^{-13}$	$0.98 \pm 0.02e^{-18}$
PHBV+10 wt %	$0.60 \pm 0.20e^{-14}$	$2.25 \pm 0.18e^{-13}$	$2.33 \pm 0.03e^{-18}$
Literature value PHBV[27]			$3.01\ e^{-18}$
Literature value PHB[28]	–	–	[b] $5.10e^{-18}$
Literature value PHB[7]	–	–	[c] $0.23e^{-18}$
PCL	$3.39 \pm 0.61e^{-14}$	$5.05 \pm 0.65e^{-13}$	$7.06e^{-18}$
PCL+1 wt. %	$1.58 \pm 0.05e^{-14}$	$4.16 \pm 1.18e^{-13}$	$5.48 \pm 0.27e^{-18}$
PCL+5 wt. %	$1.26 \pm 0.05e^{-14}$	$2.58 \pm 0.57e^{-13}$	$3.68 \pm 0.29e^{-18}$
PCL+10 wt. %	$1.26 \pm 0.05e^{-14}$	$3.80 \pm 0.57e^{-13}$	$3.67e^{-18}$
Literature value PCL	[8a] $0.023e^{-14}$	–	[30d] $1.9e^{-18}$

[a] At 35°C, 75%RH and cast from toluene.
[b] At 75%RH (commercial biobased material).
[c] At 24°C and 0%RH (obtained by melt blending).
[d] At 0%RH (solvent casting).

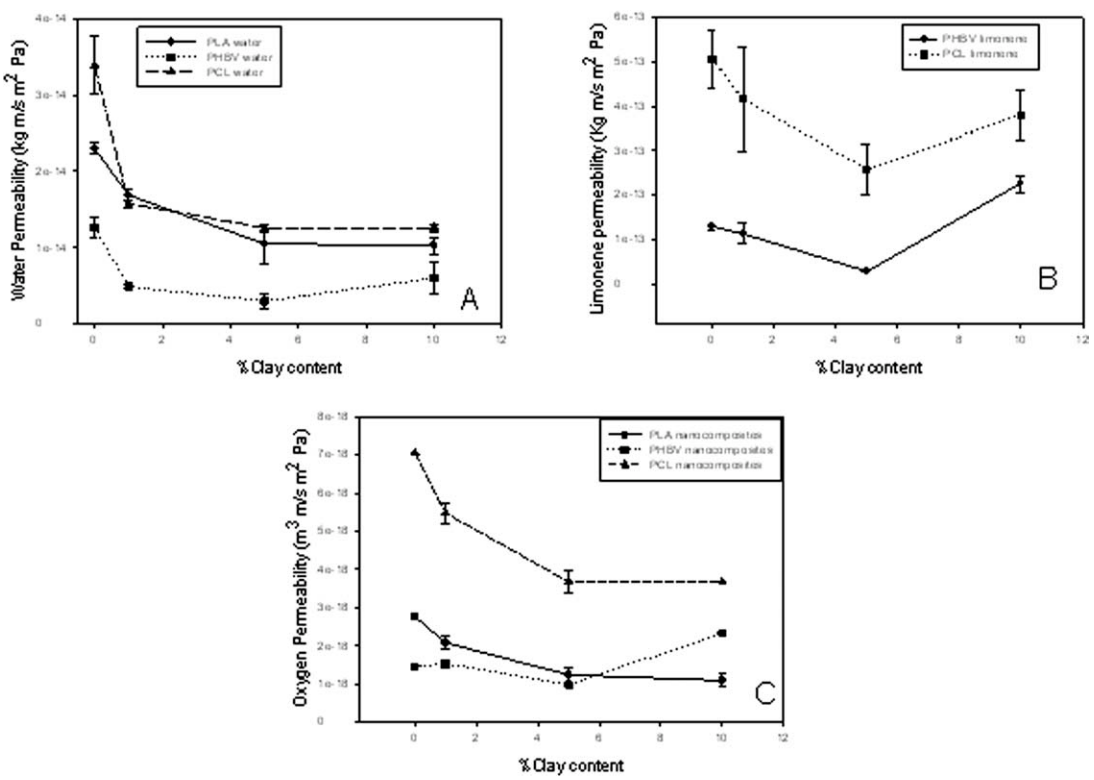

Figure 5 (A) Water permeability coefficient of PLA, PHBV, and PCL and their biocomposite with 1, 5, and 10 wt % of clay. (B) Limonene permeability coefficient of PHBV and PCL and their biocomposites with 1, 5, and 10 wt % clay content. (C) Oxygen permeability coefficient of PLA, PHBV, and PCL and their biocomposites with 1, 5, and 10 wt % clay content.

case of the PHBV, a significant reduction in limonene permeability of ca. 78% is obtained for the sample containing 5 wt % of clay loading. However, further increase in clay content until 10 wt %, does not improve the barrier as shown for other permeants above, due to clay agglomeration. Films of PCL with 1, 5 and 10 wt % of clay content have a limonene permeability decrease of 18, 49, and 25%, respectively, compared to the unfilled material. Thus, the lowest limonene permeability coefficient value is for the samples containing 5 wt % of clay in all materials. It is interesting to observe that, in general, crystallinity in the biocomposites increases by the nucleating effect promoted by the clay and, therefore, the induction of crystals as well as the nanodispersion of the clay lead to impermeable blocking elements, which promote enhanced barrier. Impermeable blocks in plastics are responsible for the increase in both detour and chain immobilization factors that enter in the denominator in the expression for the calculation of the diffusion coefficient and, therefore, result in decreased diffusion and hence in permeability. In this context, it is relevant to observe that the PHBV specimen containing 5 wt % of clay exhibits somewhat higher crystallinity compared to the 1 and 10 wt % clay containing samples and it is precisely this specimen the one showing the biggest reduction in water and limonene permeability. In any case and taking into consideration all of the earlier results, it is the combination of the optimum clay loading, i.e. in the vicinity of 5 wt %, which fills in the available free volume, and the synergetic morphological alterations generated by such loading, the responsible factors behind the reported barrier enhancement.

Table IV gathers the oxygen permeability measurements carried out in the samples. The permeability value reported in the literature for PLA of $1.75e^{-18}$ m^3m/sm^2Pa measured at 75%RH[28] is of the same order of magnitude as the value of $2.77e^{-18}m^3m/sm^2Pa$ measured in our lab at 80%RH. For the PLA composites containing 1, 5, and 10 wt % of filler content an oxygen permeability reduction of 25, 55, and 60%, respectively was observed, compared to the unfilled material [Fig. 5(C)].

For the case of the PHBV, the reported value of $5.10e^{-18}m^3m/sm^2Pa$ measured at 75%RH in the homopolymer PHB[28] is higher than the value obtained in our laboratory at 80%RH of $1.44e^{-18}m^3m/sm^2Pa$ for the copolymer PHBV. On the other hand, previous measurements carried out on melt mixed PHB followed by compression molding provided a value of $0.23e^{-18}m^3m/sm^2Pa$.[7] The variation between measurements could arise from the different material origin, i.e. homopolymer vs. copolymer, processing conditions of the two materials and the difference in the relative humidity gradient used for testing. From the current results, a reduction in oxygen permeability of 32% is measured for the film of PHBV containing 5 wt % of clay. Increasing filler content to 10 wt % does not result in further barrier increase [Fig. 5(C)].

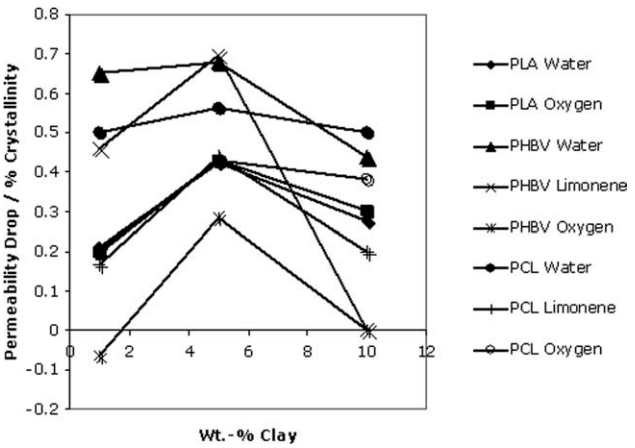

Figure 6 Clay barrier efficiency (CBE) plot for each biomaterial and permeant.

The previously reported oxygen permeability of PCL is of $1.9e^{-18}m^3m/sm^2Pa$ at 0%RH,[30] which is lower than the value of $7.06e^{-18}m^3m/sm^2Pa$ measured at 80%RH in our laboratory. The reason for the discrepancy in the absolute permeability value is again related to the different origin and processing conditions of the materials and to the difference relativity humidity used for the testing. For the PCL composites, a reduction in oxygen permeability of ca. 22, 48, and 48% was measured in the films containing 1, 5, and 10 wt % of clay content, respectively [Fig. 5(C)].

It is a general observation that composites containing 5 wt % of the filler exhibited the highest oxygen barrier performance per filler content. These results are also in good accordance, at least in relative terms, with permeability for the other permeants and with the thermal data discussed earlier, i.e. crystallinity rise due to clay-induced nucleation. The overall barrier results indicate that the barrier performance is the result of a good balance between polymer structural morphology (crystalline phase content and morphology) and filler loading. When the filler loading goes beyond the clay solubility limit in the polymer, it agglomerates and even if in some cases higher crystallinity is observed, it creates no further enhancement in barrier but in some cases an opposite behavior.

Figure 6 shows what we termed as the Clay Barrier Efficiency (CBE) for each biomaterial and permeant. This factor is calculated by dividing the penetrant permeability drop in percent between the sample %crystallinity as determined by DSC during the first heating run. This CBE factor highlights the

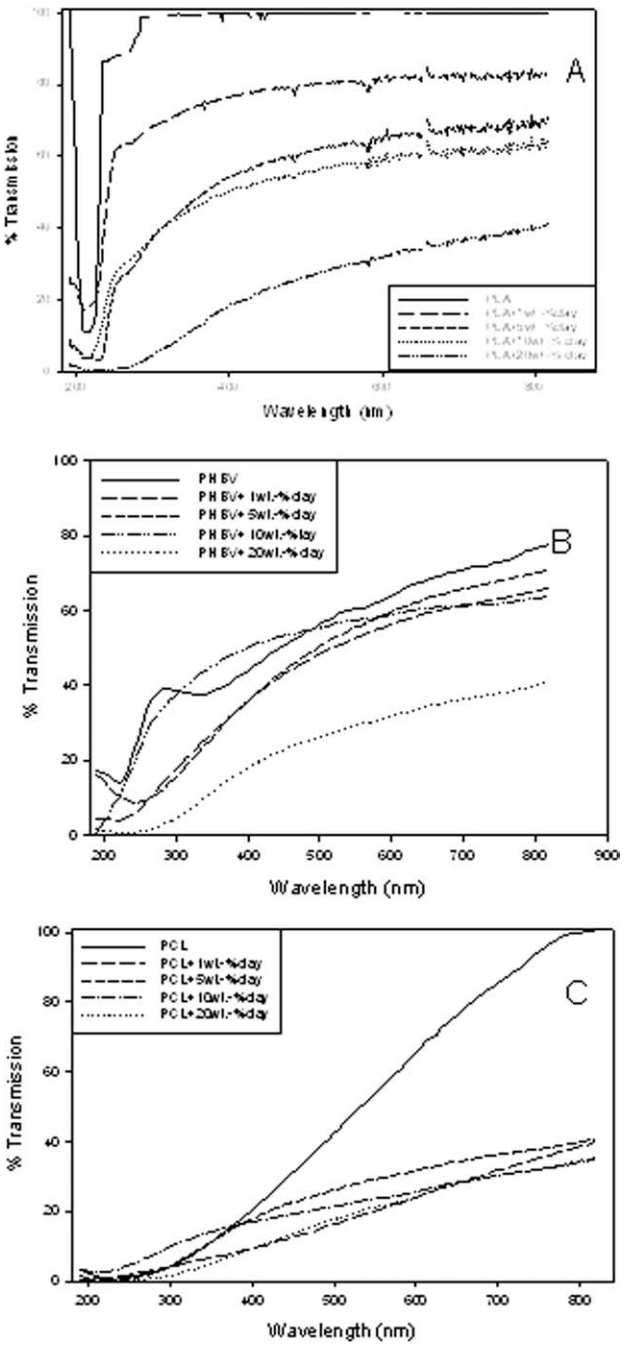

Figure 7 UV–Vis spectra normalized to 30 microns vs. clay content for cast films of PLA, PHBV, and PCL biocomposites.

barrier effect of the clay in the biomaterials and separates this from the crystallinity rise effect. From the results, the clay is more efficient at 5 wt % content for all the biomaterials tested and appears to reinforce more efficiently PHBV and PCL against water and limonene permeation and less to oxygen. It is curious to observe that in PHBV, the permeability for the biocomposite filled with 1 wt % of clay is more inefficient for oxygen than for the other biopolymers and the effect is reproducible.

UV-VIS spectra

Figure 7 shows the normalized (to 30 microns thickness) UV-Vis spectra of unfilled PLA, PHBV, and PCL and of their biocomposites. The UV region is classified in three zones: UVC (100–280 nm), UVB (280–320) and UVA (320–400 nm).

Figure 7(A) shows the transmission spectra of PLA with increasing clay content (1, 5, 10, and 20 wt % of clay). In general, the UV-Vis spectra show a reduction with increasing clay content in the films. From the results [Fig. 7(A)], the transmittance of the pure PLA in the region of UVC is of a maximum of 10%. In this range, the corresponding PLA biocomposites containing 20 wt % of clay exhibit a complete blocking to the passage of radiation. More relevant regions for protection are the UVB and UVA regions, where the pure PLA has a transmittance of around 100%, thus the PLA is virtually transparent in this range as it is in the visible range. Films of PLA containing 20 wt % of clay content reach transmission values below 15% in this region (UVB-UVA), yielding a very efficient blocking effect. The blocking effect decreases in the visible range where transparency is still highly appreciated. It is clear that 20 wt % filler content is perhaps too high a loading to be used, as it does negatively affect the transmission in the visible range and will be unlikely to yield an optimum property balance. Nevertheless, and as it was the case with the barrier performance, the ratio of protection is still very efficient at 5 wt % of clay addition, yielding 10 wt % clay loading not so much differentiating benefits. Thus, low clay contents (1 and 5 wt %) in the PLA matrix lead to significant reductions in the UV light transmission, while retaining transparency to a significant extent due to higher clay dispersion in the matrix (Table V).

In the case of PHBV, Figure 7(B) shows the transmission spectra of the biocomposites with 1, 5, 10, and 20 wt % clay content. The blocking effect of PHBV in the UV-Vis region is higher than the PLA transmission as PHBV is a translucent material. Similar as with the transmission spectra of PLA, with increasing clay content, the UV-Vis transmittance decreases to a significant extent, particularly in the

TABLE V
UV-Vis Blocking Per wt % of Clay in the PLA Biocomposite at 300 nm (UV) and 600 nm (Visible) Wavelengths

wt % clay	%T/wt % at 300 nm	%T/wt % at 600 nm
1	30.2	18.9
5	12.2	7.1
10	6.1	4.1
20	4.7	3.4

TABLE VI
Yellow Index (YI) and *L, *a*, and *b* Parameters of PLA, PHBV, PCL and of their biocomposites**

	YI	*L**	*a*	*b*
PLA	0	96.03 ± 0.13	0.37 ± 0.011	2.30 ± 0.19
PLA+1% clay	0.12	95.42 ± 0.33	0.14 ± 0.04	3.58 ± 0.10
PLA+5% clay	0.24	93.19 ± 0.26	−0.69 ± 0.05	9.63 ± 0.57
PLA+10% clay	0.21	87.29 ± 1.43	−0.71 ± 0.14	19.22 ± 1.53
PHBV	0.49	97.07 ± 0.14	−0.21 ± 0.04	3.83 ± 0.14
PHBV+1% clay	0.50	96.23 ± 0.07	−0.46 ± 0.01	6.25 ± 0.07
PHBV+5% clay	0.48	93.06 ± 1.23	−0.65 ± 0.18	9.51 ± 1.68
PHBV+10% clay	1.10	88.22 ± 0.48	−0.82 ± 0.40	22.12 ± 0.78
PCL	1.45	95.93 ± 0.27	0.10 ± 0.04	2.22 ± 0.09
PCL+1% clay	1.62	96.43 ± 0.22	−0.17 ± 0.05	4.99 ± 0.32
PCL+5% clay	0.70	93.70 ± 0.63	−0.83 ± 0.06	11.22 ± 0.83
PCL+10% clay	1.39	84.39 ± 0.63	−0.30 ± 0.06	25.10 ± 0.77

UV region, and again this is more efficient for clay contents of 5 wt %. Figure 7(C) shows the transmission spectra of PCL and of its biocomposites with different clay contents (1, 5, 10, and 20 wt %). PCL is also a very translucent material. In the UV region, the reduction in transmittance is very low compared to other biodegradable materials such as PHBV and PLA. In the visible zone, films of PCL containing 20 wt % of clay reduce transmittance to a significant extent.

As a summary, the highly transparent PLA, but also the translucent PHBV, underwent the highest UV barrier effect due to the addition of this clay. The higher barrier per filler content was observed for the 1 and 5 wt % clay content samples (Table V). Interestingly, light blocking was higher in the UV range as required and lower in the visible range for these two biopolyesters.

Table VI gathers the Yellowness Index (YI) for the biocomposites. The yellowness index describes the color changes of a sample from clear or white towards yellow. The yellowness index is dependent on the thickness of the sample; in this case the measurements were taken on 30 microns thick cast films. As it can be seen from Table VI, the YI of the PLA, PHBV, and PCL biocomposites increases with increasing filler content, and the YI data of PCL (YI = 1.5) is higher than that of PHBV (YI = 0.5) and that of PLA (YI = 0), due to the known opacity of PCL and the high transparency of the PLA.

Color measurements

The luminosity, *L**, measures the clarity at which color is perceived in the CIELAB color system. It is determined by a percentage of the light reflected by a colored object. The coordinates of chromaticity are often termed "a" and "b" in this color representation system. The coordinate "a" defines the red/green axis (+a and −a), and "b" represents the yellow/blue axis (+b and −b).

Table VI gathers the color parameters, i.e. the parameter *L** and coordinates "a" and "b", taken in the samples. From the results, the luminosity has a similar trend in all of the three biopolymers. This parameter decreased with increasing clay content as expected from all of the earlier results. The coordinate "a" decreases to negatives values with increasing clay content. Thus, films containing clay turned towards green. In the case of the coordinate "b", this value increased with increasing clay content, i.e. towards yellow. Figure 8 shows the effect on color of increasing clay content in the biocomposites for the three materials. The level of color intensifies with increasing clay content as expected but not in a linear manner. The graph shows a good correlation between color index and the optimum dispersion of the organoclay in the matrix, yielding stronger color index those biocomposites with clay loadings in excess of 5 wt %. Thus, the optical luminosity and the color of these biocomposites results primarily from addition of the clay but the level of these parameters is also related to dispersion of the clays.

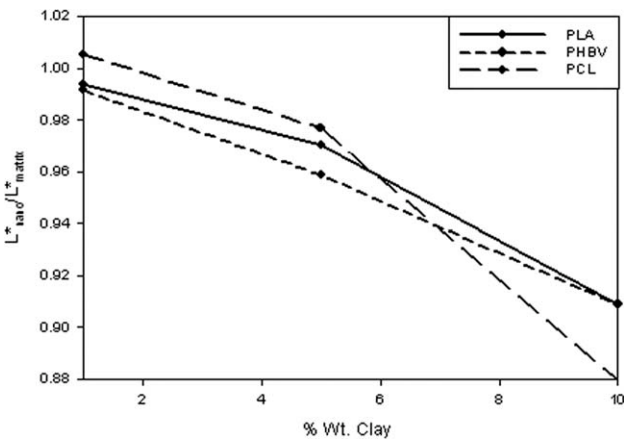

Figure 8 The effect of clay content on the biocomposites color index.

In this context, the color study is consistent with all previous data.

In summary, biocomposites of PLA, PHBV, and PCL, show a decrease in luminosity, lightness, and clarity with increasing of clay content and a change in color towards yellow and green.

CONCLUSIONS

This study successfully developed novel PHBV, PCL, and PLA-layered silicate biocomposites by a solvent casting method, wherein an organically modified mica-based filler was nicely distributed to a nanoscale level within the three biodegradable matrixes. No exfoliation of the filler was achieved in any of the matrices but in all cases extremely long platelets with thickness well in the nanoscale were observed by TEM and AFM techniques. All the biocomposites formulated exhibited improvements in properties such as gas (oxygen) and vapor (water and limonene) permeability and exhibited considerable barrier to the transmission of UV light due to the specific blocking effect of the finely dispersed mica filler. In conformity with the DSC crystallinity, which generally increased with increasing filler content, oxygen but specially water and D-limonene permeability coefficients were seen to decrease to a significant extent in the biocomposites. In the case of the barrier properties, it was observed that PLA, PHBV, and PCL containing 5 wt % of clay, led to a water permeability reduction of ca. 54, 76, and 63% and reductions in oxygen permeability of ca. 55%, 32%, and 48%, respectively, compared with the unfilled material. Reductions in limonene permeability of ca. 78% and 49%, for the films of PHBV and PCL with 5 wt % of clay were also observed. The so-called clay barrier efficiency plots, correcting for crystallinity differences, indicated that 5% was indeed the optimum clay loading, being 1% not sufficient (given the lack of exfoliation and sufficient dispersion) and 10% beyond the clay solubility limit where agglomeration and property deterioration occur. For the UV light transmission, films of PLA and PHBV with 5 wt % of clay showed a decrease in the transmission of the damaging UV light of up to ca. 75% at 250 nm wavelength. In the visible light transmission range, a reduction of ca. 32%, 10%, and 66% was observed at 650 nm wavelength for the PLA, PHBV, and PCL containing 5 wt % of clay, respectively. As a result, the increased barrier properties of the biocomposites to UV light, water, limonene and oxygen makes them potentially suitable candidates for packaging coating and membrane applications.

References

1. Van Aardt, M.; Duncan, S. E.; Marcy, J. E.; Long, T. E.; Hackney, C. R. J Dairy Sci 2001, 84, 1341.
2. Conrad, K. R.; Davidson, V. J.; Mulholland, D. L.; Britt, I. J.; Yada, S. J Food Sci 2005, 70, E19.
3. Goldhan, G.; Rieblinger, K. Eur Food Drink Rev 2002, 69. Autumn
4. Sinha Ray, S.; Yamada, K.; Okamoto, M.; Ueda, K. Polymer 2003, 44, 857.
5. Sinha Ray, S.; Yamada, K.; Okamoto, M.; Fujimoto, Y.; Ogami, A.; Ueda, K. Polymer 2003, 44, 6633.
6. Chang, J.-H; An, Y.U.; Sur, G.S. J Polym Sci Part B: Polym Phys 2003, 41, 94.
7. Sanchez-Garcia, M. D.; Gimenez, E.; Lagaron, J. M. J Appl Polym Sci 2008, 108, 2787.
8. Messersmith, P. B; Giannelis, E. P. J Polym Sci Part A: Polym Chem 1995, 33, 1047.
9. Di, Y. W.; Iannac, S.; Sanguigno, L.; Nicolais, L. Macromol Symp 2005, 228, 115.
10. Wu, T. M.; Wu, C. Y. Polym Degrad Stab 2006, 91, 2198.
11. Lee, J. H.; Lee, Y. H.; Lee, D. S.; Lee, Y. K.; Nam, J. D. Polym Korea 2005, 29, 375.
12. Petersson, L.; Oksman, K. Compos Sci Technol 2006, 66, 2187.
13. Fornes, T. D.; Yoon, P. J.; Paul, D. R. Polymer 2003, 44, 7545.
14. Yeh, J. M.; Chen, C. L.; Kuo, T. H.; Su, W. F. H.; Huang, S. Y.; Liaw, D. J.; Lu, H. Y.; Liu, C. F.; Yu, Y. H. J Appl Polym Sci 2004, 92, 1072.
15. Chaoying, W.; Yong, Z.; Yinxi, Z. Polym Test 2004, 23, 299.
16. Strawhecker, K. E.; Manias, E. Chem Mater 2000, 12, 2943.
17. Grunlan, J. C.; Grigorian, A.; Hamilton, C. B.; Mehrabi, A. R. J Appl Polym Sci 2004, 93, 1102.
18. Yoon, P. J.; Hunter, D. L.; Paul, D. R. Polymer 2003, 44, 5341.
19. Bhat, A. H.; Banthia, A. K. J Appl Polym Sci 2007, 103, 238.
20. Guo-An, W.; Cheng-Chien, W.; Chuh-Yung, C. Polym Degrad Stab 2006, 91, 2443.
21. Liu, X.; Dever, M.; Fair, N.; Benson, R. S. J Environ Polym Degrad 1997, 5, 225.
22. Barham, P. J.; Keller, A.; Otun, E. L.; Holmes, P. A. J Mater Sci 1984, 19, 2781.
23. Crank, J. The Mathematics of Diffusion; 2nd Ed.; Oxford Science Publications: Oxford, 1975.
24. Cabedo, L.; Plackett, D.; Giménez, E.; Lagarón, J. M. J Appl Polym Sci 2008, to appear; APP- 2008-03–1044.R1 Accepted.
25. Mathew, A.; Oskman, K.; Sain, M. J Appl Polym Sci 2006, 101, 300.
26. Auras, R.; Harte, B.; Selke, S. J Sci Food Agric 2005, 0022.
27. Cava, D.; Gimenez, E.; Gavara, R.; Lagaron, J. M. J Plast Films sheeting 2006, 22, 265.
28. Petersen, K.; Nielsen, P. V.; Olsen, M. B. Starch 2001, 53, 8.
29. Rhim, J.-W.; Hong, S.-I.; Ha, C.-S. Food Sci Technol 2009, 42, 612.
30. Olabarrieta, I.; Forsström, D.; Gedde, U. W.; Hedenqvist, M. S. Polymer 2001, 42, 4401.